Supplementary Materials for

Title: Electronic nematicity in Sr_2RuO_4

J. Wu[1,*], H. P. Nair[2,*], A. T. Bollinger[1], X. He[1,3], I. Robinson[1], N. J. Schreiber[2], K. M. Shen[4,5], D. G. Schlom[2,5], and I. Božović[1,3]

Correspondence to: bozovic@bnl.gov

This PDF file includes:

Materials and Methods
Supplementary Text
Figs. SF1 to SF5
Tables ST1 to ST3
Supplementary references *(SR1)-(SR10)*

www.pnas.org/cgi/doi/10.1073/pnas.1921713117

Materials and Methods

Materials

High-quality single crystal films of (001)-oriented Sr_2RuO_4 were synthesized in a Veeco GEN10 molecular-beam epitaxy system. Well-oriented 10 mm × 10 mm × 1 mm single-crystal substrates of (110) $NdGaO_3$ and (001) $(LaAlO_3)_{0.29}$–$(Sr_{1/2}Al_{1/2}TaO_3)_{0.71}$ (LSAT) from CrysTec GmbH *(31)* were heated to growth temperatures in the range 870 °C to 910 °C, as measured by an optical pyrometer operating at 1,550 nm. There they were exposed to molecular beams of strontium (99.99% purity), ruthenium (99.99% purity), and distilled ozone (~80% O_3 + 20% O_2 made from oxygen gas with 99.994% purity), all supplied at the same time (co-deposition). The strontium and ruthenium fluxes ranged from about 1.9×10^{13} to 3.3×10^{13} atoms·cm^{-2}s^{-1} and 1.4×10^{13} to 2.5×10^{13} atoms·cm^{-2}s^{-1}, respectively, corresponding to an excess ruthenium flux of about 2×10^{12} to 9×10^{12} atoms·cm^{-2}s^{-1} for the growth of Sr_2RuO_4. The growth rate of the Sr_2RuO_4 films ranged from 0.09 Å/s to 0.16 Å/s. To facilitate radiative coupling between the SiC substrate heater filament and the substrates, the back sides of the substrates were coated with a 10 nm thick titanium adhesion layer followed by 400 nm of platinum followed by 200 nm of polycrystalline $SrRuO_3$. The background oxidant pressure during growth ranged from of 8×10^{-7} Torr to 1×10^{-6} Torr. At the completion of growth, the strontium and ruthenium shutters were simultaneously closed, and the film was rapidly cooled to below 250 °C in the same pressure of distilled ozone in which it was grown. Strontium was evaporated from a low-temperature cell while an electron-beam evaporator was used for ruthenium. A typical X-ray diffraction pattern is shown in Fig. SF1, and Reflection high-energy electron diffraction (RHEED) pattern in Fig. SF2.Additional details, including the growth window for the adsorption-controlled conditions used, may be found elsewhere *(SR1)*.

The best of our Sr_2RuO_4 films are superconducting with the critical temperature $T_c \approx 1.5$ K, as high as in the best bulk Sr_2RuO_4 crystals *(SR1)*.

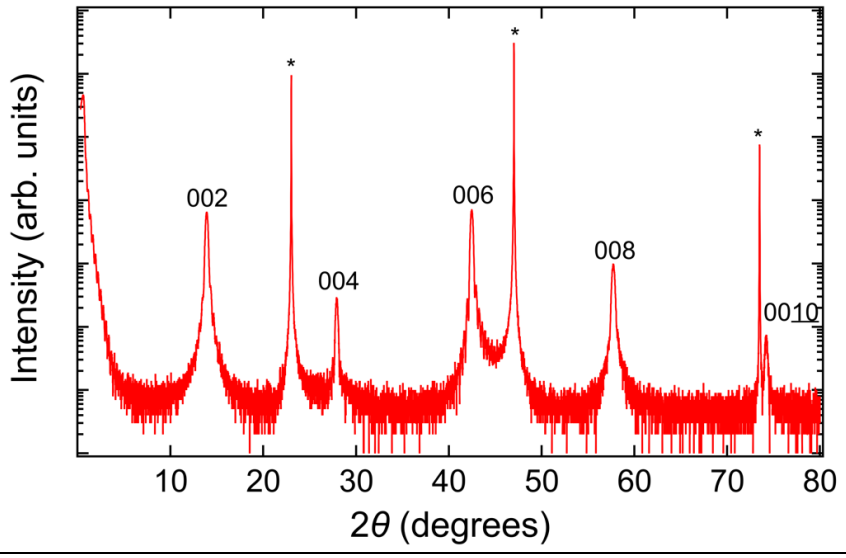

Fig. SF1. X-ray diffraction θ-2θ scan of a ~30 nm thick (001)-oriented Sr_2RuO_4 film grown on a $NdGaO_3$(110) substrate. All of the peaks in the scan can be indexed to either the film or the substrate (asterisks).

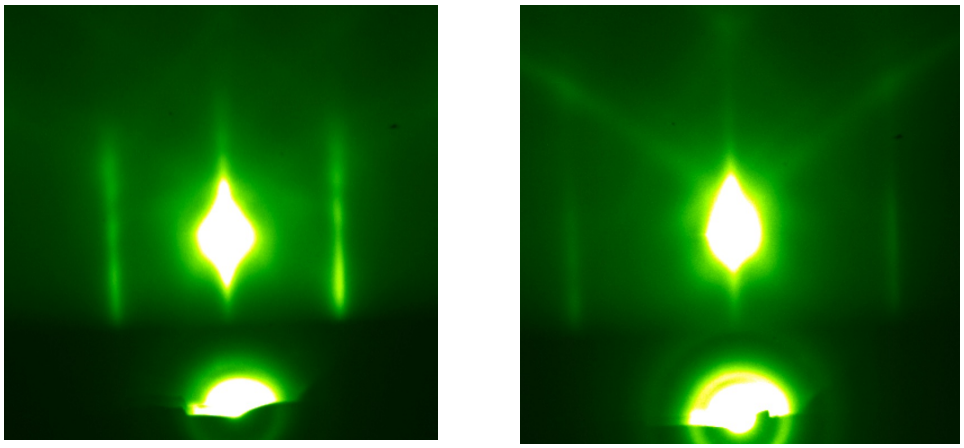

Fig. SF2. Reflection high-energy electron diffraction (RHEED) from the same film. **a,** The RHEED pattern recorded with the electron beam incident along the <100> azimuth of the Sr_2RuO_4 thin film. **b,** the same, but with the beam incident along the <110> azimuth. The RHEED patterns were recorded at a substrate temperature of 300 ˚C at the end of the growth.

Methods

The Sr_2RuO_4 films were patterned by standard photo-lithography procedures to form the "sun-beam" pattern shown in Fig. 1a in the main text. The precision in the alignment of lithography is ±1 μm. The electric current runs along a chosen Hall bar at a time with the corresponding longitudinal or transverse voltages being recorded using three pairs of evenly-spaced gold contacts (Fig. 1b) on the Hall bar. The angle $\Delta\phi$ between two successive Hall bars is 10^0 and the total of 36 Hall bars systematically map out the in-plane angle ϕ from 0^0 to 350^0. The orientation of the Hall bar with the initial angle $\phi = 0^0$ is aligned with the [100] crystal axis of Sr_2RuO_4 with a precision of 0.1^0.

The transport measurements were carried out in both Helium-4 and Helium-3 cryogenics to study the temperature dependence of longitudinal and transverse resistivity. The thermal stability of both systems is better than ±1 mK.

Supplementary Text

1. Lattice orthorhombicity determined by XRD

Single crystal X-ray diffraction was used to determine the lattice constants of the Sr_2RuO_4 films on the two substrates, $NdGaO_3$ and LSAT. An in-house Bruker D8 4-circle diffractometer was used to locate the angular positions of a number of peaks from the films using λ = 1.540 Å, 0.5 mm resolution-defining slits and a 1 mm out-of-plane detector slit to provide 3D resolution. Following the standard angle convention of Busing and Levy (*SR2)*, for each reflection the detector angle (2θ), the sample angle (θ) and the tilt Euler angle (χ) were scanned in sequence until consistent, while the azimuthal Euler angle (ϕ) was kept fixed. The peak center positions of seven accessible reflections were least-squares-fit to a general lattice without constraints to determine the lattice constants (*SR3*). The self-consistency of the fit was used to generate an absolute error, the distance in reciprocal space between the reciprocal lattice point and its measured position. These errors were then used as a conservative estimate of the accuracy of the measured lattice constants.

Tables ST1 and ST2 show the measured angles and the resulting errors for the least-squares fit. It is clear that the errors are well distributed and at the level expected for a slit-defined instrument. Table ST1 shows the measured lattice parameters of Sr_2RuO_4 films grown on LSAT substrate. The LSAT is less precisely measured, but consistent with $a = b$, or a tetragonal structure of the film. Table ST2 shows the measured lattice parameters of Sr_2RuO_4 films grown on $NdGaO_3$ substrate. The measured values of a and b for Sr_2RuO_4 on $NdGaO_3$ are no longer consistent with $a = b$, so we conclude this film to be orthorhombic.

H	K	L	2θ	θ	φ	χ	Error (Å^{-1})
1	-1	4	43.50	21.760	-46.26	40.61	0.0039
-1	1	4	43.50	21.761	133.51	40.64	0.0039
-1	-1	4	43.51	21.770	223.52	40.76	0.0025
1	1	4	43.53	21.766	43.71	40.50	0.0047
0	1	3	31.23	15.619	88.60	42.46	0.0067
-1	0	3	31.23	15.622	178.45	42.53	0.0045
1	0	3	31.23	15.619	-1.21	42.41	0.0055

Table ST1. The measured diffractometer angles and the resulting errors to the least-squares fit for Sr_2RuO_4 films on LSAT.

H	K	L	2θ	θ	φ	χ	Error (Å^{-1})
-1	0	3	31.31	15.566	225.50	42.11	0.0020
0	1	3	31.22	15.607	135.51	42.12	0.0030
1	0	3	31.31	15.649	45.65	42.05	0.0025
0	-1	3	31.26	15.614	-44.44	42.36	0.0036

1	1	4	43.55	21.787	90.50	40.37	0.0021
-1	1	4	43.58	21.771	180.46	40.34	0.0037
1	-1	4	43.56	21.787	0.73	40.45	0.0038

Table ST2. The measured diffractometer angles and the resulting errors to the least-squares fit for Sr_2RuO_4 films on $NdGaO_3$.

Substrate	a	b	c	α	β	γ	Volume (Å^3)
LSAT	3.873(11)	3.874(11)	12.75(4)	90.09	89.98	90.01	190
$NdGaO_3$	3.848(7)	3.861(7)	12.79(2)	90.00	89.99	89.95	191

Table ST3. Measured lattice parameters of Sr_2RuO_4 films on the two different substrates. Errors estimated from the misfit of the lattice are shown in parentheses.

2. Pitfalls of using the van der Pauw method to probe nematicity

The van der Pauw method is commonly used to measure the resistivity of single crystals. This method, as it was originally conceived and most widely utilized (*SR4*) is appropriate for measuring the resistivity of materials with isotropic in-plane conductivity. For materials with anisotropic resistivity, e.g., when it is desired to probe for electronic nematicity, this approach has pitfalls of which one should be aware (*SR5,SR6*). Below is an example that illustrates the subtlety.

On a uniform as-grown Sr_2RuO_4 film on an (110) $NdGaO_3$ substrate, four point contacts were wire-bonded onto the four corners to carry out the van der Pauw measurements. The recorded $R(T)$ along two orthogonal directions [001] and $[1\bar{1}0]$ manifest significant difference (Fig. SF3a), confirming $R_a \neq R_b$ and consequently the nematicity. Intuitively, one would expect that the magnitude of the nematicity N should be proportional to ΔR ($= R_a - R_b$). If that were true, N should first decrease with sample cooling until it vanishes at $T \sim 40$ K, and on further cooling N should increase, but with the opposite sign. This inferred peculiar $N(T)$ behavior is, however, merely an artifact due to misinterpretation of the van der Pauw method. To illustrate this, we patterned the same Sr_2RuO_4 film with the sun-beam lithography pattern (Fig. 1a) and measured the longitudinal resistivity ρ along the same [001] and $[1\bar{1}0]$ directions. One can see that $\rho_a \neq \rho_b$, i.e., the electronic state is nematic, consistent with Fig. SF3a. Remarkably, the $\rho_a(T)$ and ρ_b T) do not cross at any T from 295 K down to 4 K (Fig. SF3b). The calculated $N(T)$ does not change sign at any temperature; it monotonically increases as T decreases, similar to $N(T)$ shown in Fig. 3.

The merit of the sun-beam method is that the excitation current is guided by the Hall bar geometry to run uniformly along a given direction (*SR7*). Conversely, in the van der Pauw method, the current density $\boldsymbol{j}$ between two current contacts varies locally in both direction and amplitude. More importantly, the spatial distribution of $\boldsymbol{j}$ is susceptible to the magnitude of the nematicity. Thus, the correct interpretation of the measured R_a and R_b demands a delicate self-consistent modeling of $\boldsymbol{j}$ under the influence of the unknown N. It is clear that the dependence of R on N can be approximated as a collinear function only under the extreme condition if N is so tiny that the

influence of the nematicity is negligible to ***j*** and the usual van der Pauw analysis applies. Generally, R does not bear a simple relation to N.

We note that van der Pauw (*SR5*), Montgomery (*SR6*) and others recognized this limitation and developed variants of the original van der Pauw method that are appropriate for measuring electronic nematicity. Unfortunately, these latter methods require either six planar samples of known and distinct orientation (*SR5*) or *a priori* knowledge of the principal axes (*SR6*), making them inappropriate for a study of a single thin film.

Nevertheless, we applied this method to analyze the resistance data shown in Fig. SF3a and calculated the longitudinal resistivity along the same [001] and $[1\bar{1}0]$ directions respectively (Fig. SF3c). The two $\rho(T)$ curves plotted in Fig. SF3c show no crossings, in stark contrast to the two R(T) curves in Fig. SF3a, but in qualitative agreement with the $\rho(T)$ curves in Fig. SF3b. This confirms that the crossing in Fig. SF3a is merely an artifact, due to the fact that the principal axes are not aligned with either the a or b axes. The quantitative values of $\rho(T)$ in Fig. SF3c at a fixed temperature, e.g. T = 295 K, are fairly close to those of $\rho(T)$ in Fig. SF3b. The magnitude of the nematicity, determined by the difference between the two $\rho(T)$ curves, are nearly the same in Fig. SF3b and Fig. SF3c at 4.2 K, but gets underestimated in Fig. SF3c at elevated temperatures.

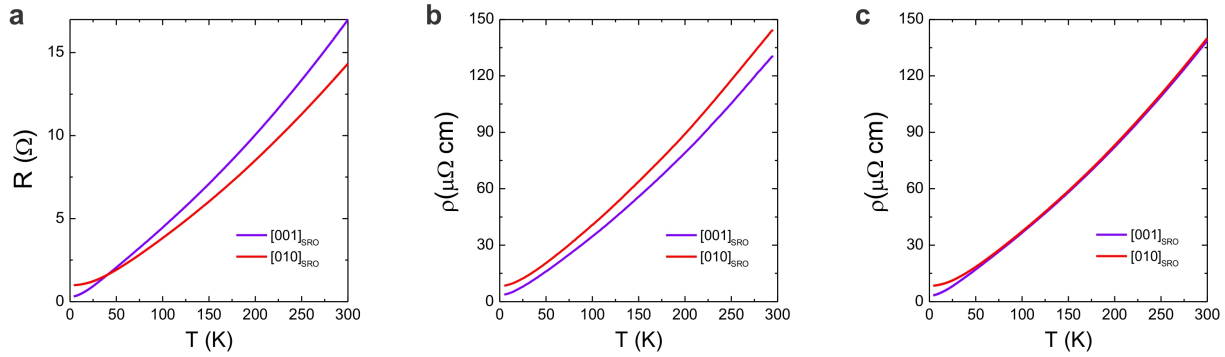

Fig. SF3. A comparison of the van der Pauw and the sunbeam-pattern methods. **a,** The longitudinal resistances of Sr_2RuO_4 grown on (110) $NdGaO_3$ were measured along [001] and $[1\bar{1}0]$ directions of $NdGaO_3$ respectively, by the van der Pauw method. **b,** On the same sample after being patterned by the sun-beam lithography pattern, the longitudinal resistivities were again measured. **c**, The longitudinal resistivity along [001] and $[1\bar{1}0]$ were calculated from the resistance data in **a**, based on the van der Pauw method generalized to anisotropic materials (*43*).

To avoid the complexity in analysis and modeling, the sun-beam method is clearly preferable. Moreover, for the more general case in which the principal axes do not align with the crystal a or b axis, e.g., in Sr_2RuO_4 films grown on LSAT (Fig. 1), the interpretation of the van der Pauw method gets less straightforward. For instance, if a principal axis is along the [110] direction of Sr_2RuO_4, then the measured $R_a = R_b$, misleading one to infer that the nematicity is zero. Therefore, the angular resolution of the sun-beam method is pivotal to ensure the accurate characterization of nematicity.

3. Robustness of superconductivity and electronic nematicity

The electronic nematicity is present in Sr_2RuO_4 films on both LSAT and $NdGaO_3$ substrates at room temperature and its magnitude increases with decreasing temperature. For the Sr_2RuO_4 film grown on a (110) $NdGaO_3$ substrate, superconductivity was observed at low temperatures with the onset T_c = 0.9 K (Fig. SF4a). By adjusting the growth condition slightly off the optimal, we introduced more defects into the film and suppressed superconductivity so that no transition is observed (Fig. SF4c) down to 0.3 K. On the other hand, the angular dependence of $\rho_T(\phi)$ of both films manifest 180^0 oscillations and possess a very similar "clover-leaf" shape when plotted in polar coordinates (Figs. SF4b and SF4d). This comparison clearly shows that the electronic nematicity in the normal state of Sr_2RuO_4 is robust against the disturbance caused by structural defects and the demise of the superconductivity. Nematicity, or a large nematic susceptibility, appears to be intrinsic to Sr_2RuO_4.

4. The substrate miscut is not the root cause of the observed nematicity

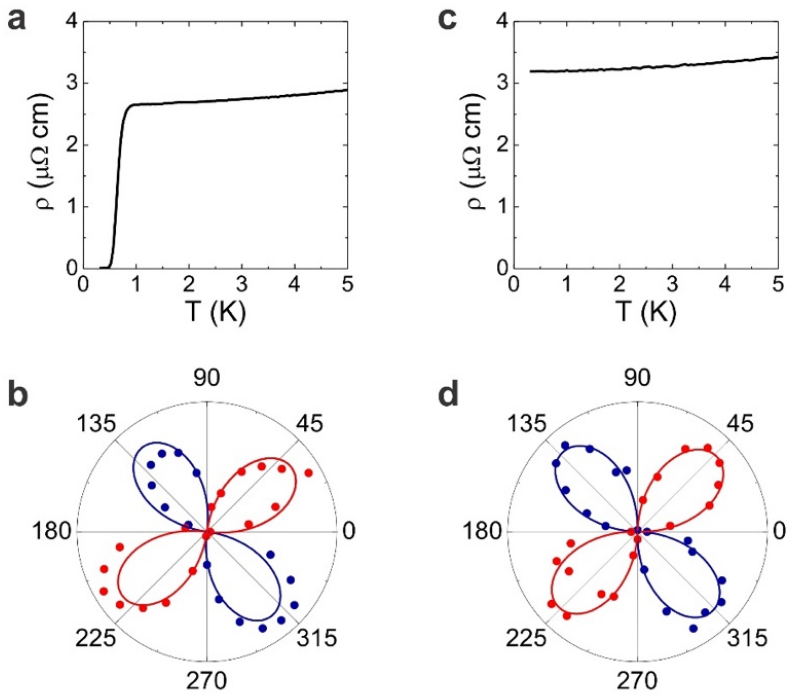

Fig. SF4. **The magnitude of nematicity is nearly the same in superconducting and non-superconducting Sr_2RuO_4 films.** **a,** the longitudinal resistivity $\rho(T)$ shows superconductivity with $T_c \approx 0.9$ K. **b,** $\rho_T(\phi)$ at T = 295 K in the same sample, plotted in polar coordinates. **c,** $\rho(T)$ of a non-superconducting film with a higher residual resistivity. **d,** $\rho_T(\phi)$ of the non-superconducting film.

Restricted by the precision in the alignment during polishing, the surface of a substrate, e.g. LSAT, inevitably deviates from the ideal crystallographic {001} plane by a tiny miscut angle. The upper limit of the miscut for the substrates used is 0.2 degree. The atomic steps at the Sr_2RuO_4/LSAT and Sr_2RuO_4/$NdGaO_3$ interfaces, and the concomitant out-of-phase boundaries in the Sr_2RuO_4 film (*SF8*), in principle violate the $\mathbf{C}_4$ rotational symmetry. Traversing the steps and out-of-phase boundaries can increase the electronic scattering rate, so the in-plane resistivity could be larger in

that direction. In addition, note that Sr_2RuO_4 is a layered material and has a considerable in-plane vs. out-of-plane anisotropy so one could also increase the measured resistivity in the direction perpendicular to the substrate steps by picking up some *c*-axis component. If this were indeed the case, there should be a one-to-one correspondence between the step orientation and the orientation of the principal axes; resistivity should always be the lowest in the direction parallel to the steps.

This motivated us to explore whether the orientation and density of the atomic steps are related to the measured anisotropy in the Sr_2RuO_4 films. Since the miscut varies randomly from one substrate to another, the resulting atomic steps vary in density and orientation. By choosing substrates with different miscut and synthesizing Sr_2RuO_4 films under identical conditions, we can make a one-on-one comparison between the orientation of the anisotropy and the miscut. Since traversing the steps and out-of-phase boundaries can only increase the electronic scattering rate, and consequently the longitudinal resistivity, the in-plane direction parallel to the atomic steps should correspond to the direction in which the resistivity $\rho(\phi)$ reaches its minimum ρ^{min}.

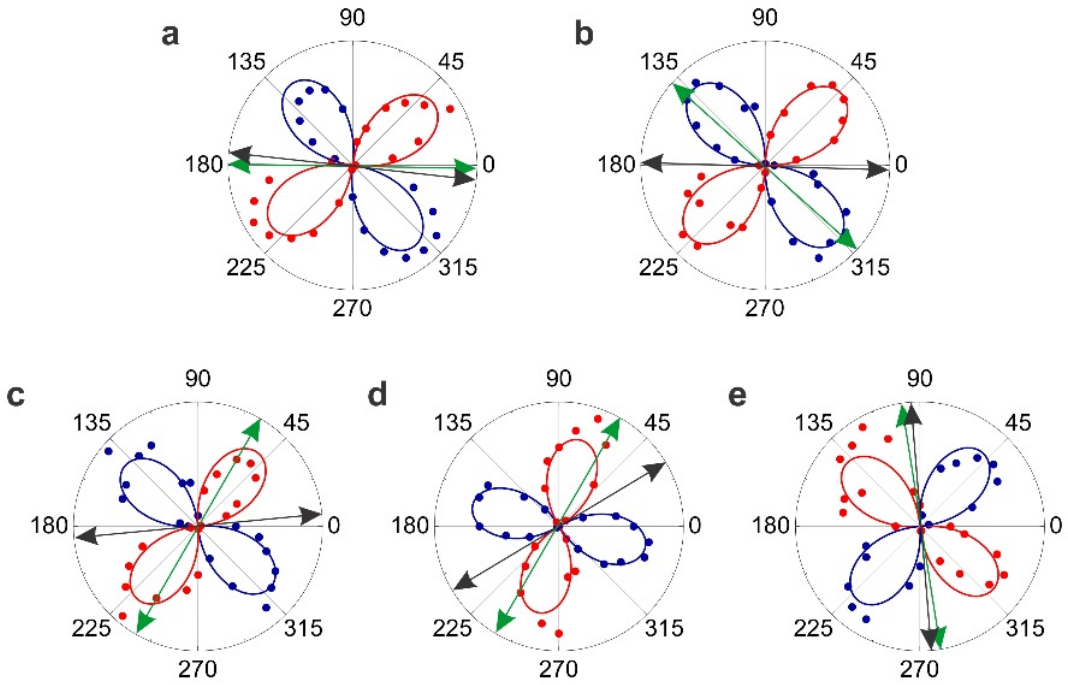

Fig. SF5. In Sr_2RuO_4 films grown on (110) $NdGaO_3$ under identical growth conditions, the orientation of substrate steps (green arrows) does not coincide with the principal axis along which the resistivity is lowest (black arrows). a, The miscut angle of the substrate is $\theta = 0.05^0$. **b,** $\theta = 0.06^0$. **c,** $\theta = 0.038\pm0.001^0$. **d,** $\theta = 0.140\pm0.002^0$. **e,** $\theta = 0.16\pm0.01^0$. The horizontal axis in all plots is along the direction with [001] the shorter lattice constant of the perovskite subcell in the $NdGaO_3$ substrate and the shorter in-plane lattice constant of the Sr_2RuO_4 film.

The direction and magnitude of the substrate miscut was measured by XRD using the technique outlined in Ref. *SR9*. In Fig. SF5, we show the measured orientation of the atomic steps, denoted by the green arrows, for five Sr_2RuO_4 films grown on (110) $NdGaO_3$ substrates. (The horizontal

axis in all plots is aligned with the [001] axis of $NdGaO_3$, i.e., it is in the direction with the shorter lattice constant of the perovskite subcell in the $NdGaO_3$ substrate and the shorter in-plane lattice constant of Sr_2RuO_4 film.) For comparison, the orientation of the principal axis along which the resistivity is lowest, i.e., the angle corresponding to $\rho^{min}(\phi)$, is indicated by the black arrows. It is clear there is no one-to-one correspondence between the orientations of substrate steps and the direction of ρ^{min} (which would correspond to the nematic director).

Moreover, an even stronger argument against this model is its dramatic failure to account quantitatively for the magnitude of the observed effect. In principle, given the large out-of-plane vs. in-plane resistivity anisotropy in Sr_2RuO_4 (of the order of 1,000:1), the substrate miscut could cause some admixture of the *c*-axis resistivity if the current is running along the miscut direction. To estimate the magnitude of this effect, one needs to know the miscut angles, so these were measured and are indicated in the caption to Fig. SF5 for each of the five films. The smallest of these is $\theta = 0.038 \pm 0.001^0$ (Fig. SF5c) and in this case, the 'step model' would predict $N = 0.03\%$, three orders of magnitude less than what we see. And even for the largest miscut value, $\theta = 0.16 \pm 0.01^0$ (Fig. SF5e), the predicted N would be less than 1%, still too low by a factor of 40. The details of this quantitative comparison are provided below.

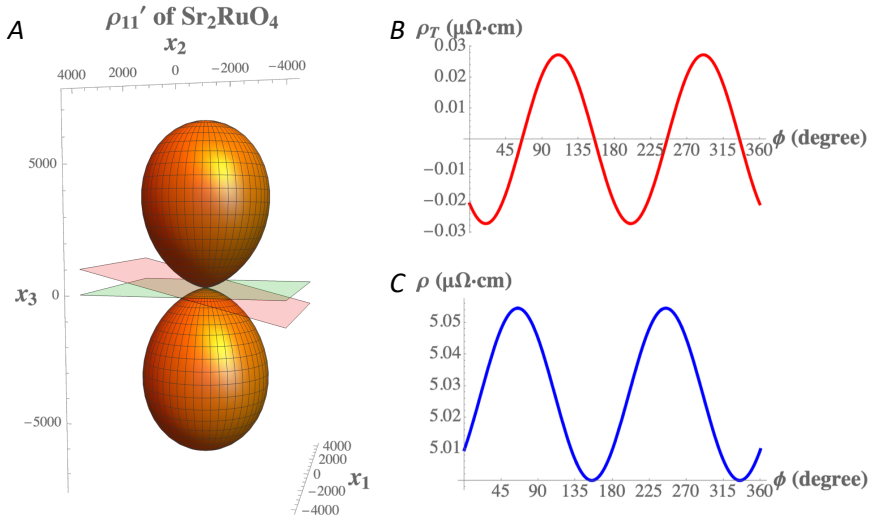

Fig. SF6. Calculated effect of the misorientation of the substrate on $\rho_T(\phi)$ and $\rho(\phi)$. (*A*) the calculated longitudinal resistivity of Sr_2RuO_4 in units of μΩ·cm. The green plane shows how a substrate precisely parallel to (001) would cut this figure; the case for a misoriented substrate is depicted by the red plane. The calculated transverse resistivity (*B*) and longitudinal resistivity (*C*) in a plane misoriented by 0.16^0 from (001).

In this analysis we assume that Sr_2RuO_4 is not an electronic nematic and calculate the angular dependence of the longitudinal resistivity ($\rho(\phi)$ or ρ'_{11} in tensor form) and transverse resistivity ($\rho_T(\phi)$ or ρ'_{21} in tensor form) expected in a perfect epitaxial (001)-oriented Sr_2RuO_4 film due solely to a miscut of the underlying substrate. With space group $I\frac{4}{m}mm$ (*36*), the form of the resistivity tensor for Sr_2RuO_4 is $\rho_{ij} = \begin{pmatrix} \rho_{11} & 0 & 0 \\ 0 & \rho_{11} & 0 \\ 0 & 0 & \rho_{33} \end{pmatrix}$. At ~8 K, $\rho_{11} \approx 1\ \mu\Omega \cdot \text{cm}$ and $\rho_{33} \approx$

$1{,}400\ \mu\Omega \cdot \text{cm}$ in Sr_2RuO_4 single crystals and for temperatures < 20 K the ratio of $\frac{\rho_{33}}{\rho_{11}}$ is approximately constant with a value of 1,400. *(SR10)* In the calculation that follows we use $\rho_{11} \approx 5\ \mu\Omega \cdot \text{cm}$ and $\rho_{33} \approx 5 \times 1{,}400 = 7{,}000\ \mu\Omega \cdot \text{cm}$ for Sr_2RuO_4 to make the results easy to compare to Fig. 1*E* and *F* and Fig. 2*C* and *D*. These higher values of ρ_{11} and ρ_{33} can be considered to result from increased disorder or a higher temperature — about 32 K for the Sr_2RuO_4 single crystal. *(10)* The quantitative effect of misorientation on the magnitude of *N* depends solely on the ratio of ρ_{33} to ρ_{11}.

The anisotropy of the longitudinal resistivity of Sr_2RuO_4 over all directions, not just those in the (001) plane, can be seen by plotting $\rho'_{11}(\theta, \phi)$ as a function of spherical angles θ and ϕ. This is achieved using the tensor equation $\rho'_{ij} = a_{ik}a_{j\ell}\rho_{k\ell}$ with $a_{11} = \sin(\theta)\cos(\phi)$, $a_{12} = \sin(\theta)\sin(\phi)$, and $a_{13} = \cos(\theta)$. A three-dimensional plot of the longitudinal resistivity, $\rho'_{11}(\theta, \phi)$, of Sr_2RuO_4 plotted as a function of direction with respect to unit vectors x_1, x_2, and x_3 parallel to the crystallographic axes *a*, *b*, and *c*, respectively, is shown in Fig. SF6*A*. It is evident that the anisotropy in Sr_2RuO_4 is very high and this is why utilizing well-oriented substrates and precisely establishing their misorientation is so important in this study. For a perfectly oriented (001) substrate, illustrated in Fig. SF6*A* by the green plane, the longitudinal resistivity in the (001) plane of the substrate would be a perfect circle and the transverse resistivity would be zero. When the substrate is misoriented, as schematically indicated in Fig. SF6*A* by the red plane, the in-plane resistivity becomes peanut shaped with principal axes aligned along the direction of misorientation. This is accompanied by the transverse resistivity becoming non-zero. The calculated dependence of the transverse resistivity, $\rho_T(\phi)$, and longitudinal resistivity, $\rho(\phi)$, in the plane of a Sr_2RuO_4 film that is misoriented by 0.16^0 from (001) are shown in Figs. SF6*B* and *C*, respectively. It is evident that the magnitude of the calculated angular dependence is far smaller than the experimentally observed angular dependence seen in Fig. 1*E* and *F* and Fig. 2*C* and *D*.

5. Temperature dependence of ρ and ρ_T

Representative plots of the temperature dependence of ρ and ρ_T for the Sr_2RuO_4 film grown on LSAT substrate are shown in Fig. SF7. The three angles ϕ are chosen so that $\rho(\phi)$ is at the maximum (70^0), middle (110^0), and minimum (160^0), see Fig. 1d and 1f for the $\rho(\phi)$ plot. It is clear from Fig. SF7 that $\rho(T)$ is parabolic, in contrast to the nearly-linear $\rho_T(T)$ behavior. This difference is also illustrated in Fig. SF7c. Apparently, the ratio ρ/ρ_T is not constant, unambiguously showing that ρ and ρ_T are two independent physical quantities.

The correlation between ρ and ρ_T is given by the equations (1) and (2) in the main text. One consequence following these equations is the prediction that $\rho_T{}^0 = \Delta\rho = (\rho_{max} - \rho_{min})/2$. Here, at every temperature, $\rho_{max} = \rho(\phi = 70^0)$ and $\rho_{min} = \rho(\phi = 160^0)$, respectively. Meanwhile, $\rho_T{}^0$ corresponds to $\phi = 110^0$, the angle at which $\rho(\phi)$ reaches the average $\bar{\rho}$ while $\rho_T(\phi)$ reaches the maximum (see Fig. 1 in the main text). Therefore, it can be inferred that $\rho_T(\phi = 110^0) = (\rho(\phi = 70^0) - \rho(\phi = 160^0))/2$. Indeed, this non-trivial relation is clearly confirmed in Fig. SF7d. This is additional strong evidence that the unusual transverse resistivity ρ_T originates from the electronic nematicity.

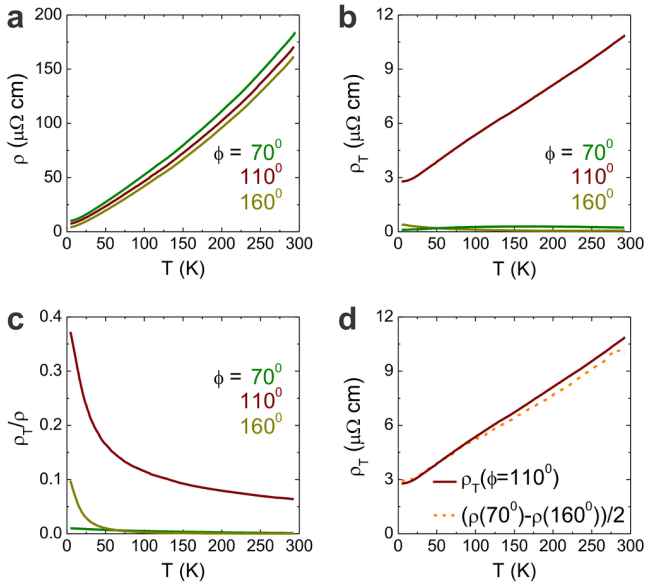

Fig. SF7. Temperature dependence of ρ and ρ_T of the Sr_2RuO_4 film on LSAT substrate. **a,** the longitudinal resistivity $\rho(T)$ at three angles corresponding to the maximum (70^0), middle (110^0), and minimum (160^0) of $\rho(\phi)$. **b,** $\rho_T(T)$ at these three angles. **c,** the ratio ρ/ρ_T is not a constant, showing that ρ_T is indeed not proportional to ρ, thus ruling out the possibility that the observed transverse voltage is due to misalignment of the voltage contacts. **d,** $\rho_T(\phi=110^0)$ is essentially equal to $(\rho_T(\phi=70^0) - \rho_T(\phi=160^0))/2$, as expected from equations (1) and (2). This shows that the origin of the transverse voltage is the anisotropy of ρ(T), i.e., the actual or incipient electronic nematicity.

6. Ruling out the artifacts of lithography: $\rho_T(\phi)$ in the control-sample Ti film

In order to test the (unlikely) possibility that our lithography and measurements may be the cause of the observed angular oscillations in $\rho_T(\phi)$, we performed a full ARTR study of a thin Ti film, chosen as a control sample. Ti is a well-known conventional metal and should not be an electronic nematic. Thus, for the Ti film, $\rho_T(\phi)$ should not oscillate with ϕ; rather, it should be zero at every angle, by symmetry. Whether or not this is observed in our experiments is a decisive test of our ARTR methodology and of any artifacts due to lithography and measurement technique.

A 16 nm thick polycrystalline Ti film was deposited on (001) Si substrate by e-beam evaporation and patterned by the standard photolithography to form the sun-beam pattern as shown in Figs. 1a and 1b in the main text. ARTR measurements were carried out on the patterned Ti film, following exactly the same procedure as for the Sr_2RuO_4 films, in particular using the same lithography mask and the same measurement setup. To compare Ti and Sr_2RuO_4 films on the same footing, we normalized the measured $\rho_T(\phi)$ by the corresponding average longitudinal resistivity $\bar{\rho}$ for Ti and Sr_2RuO_4 films, respectively. The results are shown in Fig. SF8. Apparently, $\rho_T(\phi)$ in the Ti film shows no oscillations and is equal to zero within the experimental uncertainty. This is in stark contrast to $\rho_T(\phi)$ in the Sr_2RuO_4 film. Therefore, it seems quite definite that our lithography and measurement methodology are not the cause of the observed breaking of the rotational symmetry in Sr_2RuO_4 films.

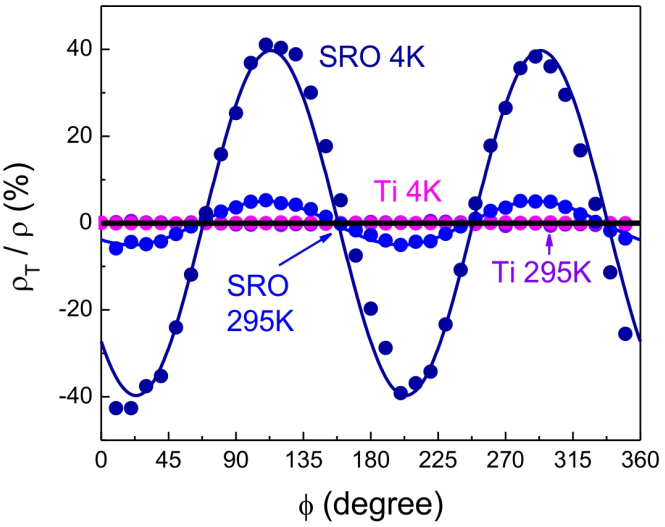

Fig. SF8. **Comparison of Sr_2RuO_4 with the Ti control sample.** In Ti film, $\rho_T(\phi)$ shows no angular oscillations at $T = 295$ K (purple dots) nor at $T = 4$ K (magenta dots). This is in stark contrast to $\rho_T(\phi)$ of the Sr_2RuO_4 film grown on the LSAT substrate ($T = 295$ K, lighter blue dots; $T = 4$ K, darker blue dots). The measured $\rho_T(\phi)$ is normalized by the average longitudinal resistivity $\bar{\rho}$ for the respective films, in order to facilitate the comparison. The solid lines are the best fits to $\rho_T(\phi) = \rho_T^0 \sin[2(\phi-\alpha)]$ for experimental data in the corresponding color. The solid black line stands for $\rho_T(\phi)/\bar{\rho} = 0$.

Supplementary references

1. H. P. Nair *et al.*, Demystifying the growth of superconducting Sr_2RuO_4 thin films. *APL Materials* **6**, 101108 (2018).
2. W. R. Busing, H. A. Levy, Angle calculations for 3- and 4- circle X-ray and neutron diffractometers. *Acta Cryst.* **22**, 457 (1967).
3. Chinkyo Kim, "Strain Relaxation Mechanism of Semiconductor Thin Films." PhD Thesis, University of Illinois, Urbana (1998).
4. L. J. van der Pauw, A method of measuring specific resistivity and Hall effect of discs of arbitrary shape. *Philips Res. Rep.* **20**, 220–224 (1958).
5. L. J. van der Pauw, Determination of resistivity tensor and Hall tensor of anisotropic conductors. *Philips Res. Rep.* **16**, 187–195 (1961).
6. H. C. Montgomery, Method for measuring electrical resistivity of anisotropic materials. *J. Appl. Phys.* **42,** 2971–2975 (1971).
7. J. Wu, A.T. Bollinger, X. He, I. Božović, Spontaneous breaking of rotational symmetry in copper oxide superconductors. *Nature* **547**, 432-435 (2017).
8. M. A. Zurbuchen *et al.*, Morphology, structure, and nucleation of out-of-phase boundaries (OPBs) in epitaxial films of layered oxides. *J. Mater. Res.* **22** 1439–1471 (2007).

9. M. A. G. Halliwell, S. J. Chua, Determining substrate orientation using a high-resolution diffractometer. *Journal of Crystal Growth* **192**, 456-461 (1998).

10. N. E. Hussey, A. P. MacKenzie, J. R. Cooper, Y. Maeno, S. Nishizaki, and T. Fujita, Normal-state magnetoresistance of Sr_2RuO_4. *Physical Review B* **57**, 5505–5511 (1998).